Chemical Engineering Journal 180 (2012) 237–244

Contents lists available at SciVerse ScienceDirect

Chemical Engineering Journal

journal homepage: www.elsevier.com/locate/cej

Linear growth rate of nanosized calcite synthesized via gas–solid carbonation of $Ca(OH)_2$ particles in a static bed reactor

G. Montes-Hernandez[a,*], D. Daval[b,c,1], N. Findling[a,b], R. Chiriac[d], F. Renard[a,e]

[a] CNRS and University Joseph Fourier-Grenoble 1, Institut des Sciences de la Terre (ISTerre), OSUG/INSU, BP 53, 38042 Grenoble, Cedex 9, France
[b] UMR 8538, Ecole Normale Supérieure, 24 Rue Lhomond, 75231 Paris Cedex 5, France
[c] Laboratoire d'Hydrologie et de Géochimie de Strasbourg, Université de Strasbourg/EOST-CNRS UMR 7517, 1 Rue Blessig, 67084 Strasbourg, France
[d] Université de Lyon, Université Lyon 1, Laboratoire des Multimatériaux et Interfaces UMR CNRS 5615, 43 bd du 11 novembre 1918, 69622 Villeurbanne, Cedex, France
[e] Physics of Geological Processes, University of Oslo, Norway

ARTICLE INFO

Article history:
Received 27 November 2010
Received in revised form 7 November 2011
Accepted 8 November 2011

Keywords:
Gas–solid carbonation
Portlandite
Nanosized calcite
Linear growth rate
Mass growth rate
Rietveld refinement method

ABSTRACT

The linear growth rate is an essential parameter to describe and simulate the crystal growth processes of solid materials. In the present study, two independent methods were used to estimate how calcite particle size was increasing with reaction time. First, a direct method by using Rietveld refinements of X-ray diffraction patterns quantifies the variation of the coherent domain average size r with reaction time t. Second, we used a mass balance method where the formed calcite amount $Mol_{CaCO_3,t}$ was determined as a function of time and the linear growth rate was deduced from mass growth rate. For both methods, a kinetic pseudo-second-order expression was successfully used to fit the data and estimate the initial growth rates of nanosized calcite. The results deduced from Rietveld refinements showed that such rates were roughly equivalent for two different temperature conditions, i.e. 0.35 nm/s at 30 °C and 20 bar, and 0.27 nm/s at 60 °C and 20 bar. However, these results were significantly different from those deduced from mass growth rate. For this case, values of 0.09 nm/s at 30 °C and 20 bar, and 0.06 nm/s at 60 °C and 20 bar were determined. This significant discrepancy could be ascribed to other simultaneous processes during crystal growth of calcite such as agglomeration and possibly dissolution–reprecipitation reactions, complicating considerably the measurement of linear growth rate by mass balance. The latter process was possibly enhanced by the release of water into the reactor during the gas–solid carbonation reaction ($Ca(OH)_2 + CO_2 \rightarrow CaCO_3 + H_2O$), and suggested to be experimentally evidenced for reaction extents greater than 80%. Taken together, these results suggest that the method based on Rietveld refinements may be more reliable to determine initial linear growth rates for reactions initiated in biphasic (gas–solid) systems, whereas both methods were previously demonstrated to be equivalent for triphasic systems.

1. Introduction

The gas–solid carbonation processes using alkaline sorbents are of growing interest because of their potential to capture CO_2 via non-catalytic exothermic reactions, allowing the selective mineralization of CO_2 from a complex mixture of several gases. Recently, it was demonstrated that nanosized portlandite ($Ca(OH)_2$) can be completely transformed into nanosized calcite (<100 nm) via gas–solid carbonation under moderate CO_2 pressure (<40 bar) and low temperature (<60 °C). For this case, the mineralization of CO_2 does not form a protective carbonate layer around the reacting particles of portlandite as typically observed by other carbonation methods (e.g. [1–5]). For this reason, the gas–solid carbonation of portlandite could be efficiently performed to produce nanosized calcite with high potential for industrial applications (e.g. filler in papermaking industry and printing inks, antacid tablets, adsorbents etc.). Nanosized calcite particles with low aggregation and agglomeration states could actually offer better dispersion when they are used as additive in printing inks or better particle distribution when they are used as a brightness additive in cellulose fibres for paper fabrication. Nanosized calcite particles are whished as well for antacid tablets because their dissolution is faster than that of microsized particles. Moreover, the separation of solid product from fluid phase is simpler than in precipitation methods [6]. The present study is particularly focused on the kinetic behaviour of calcite growth in order to determine the linear growth initial-rate, an essential parameter to be used in predictive models to simulate the nucleation and growth processes of minerals and solid

* Corresponding author.
E-mail address: german.montes-hernandez@obs.ujf-grenoble.fr (G. Montes-Hernandez).
[1] Present address: Laboratoire d'Hydrologie et de Géochimie de Strasbourg, Université de Strasbourg/EOST-CNRS UMR 7517, 1 Rue Blessig, 67084 Strasbourg, France.

1385-8947/$ – see front matter © 2011 Elsevier B.V. All rights reserved.
doi:10.1016/j.cej.2011.11.020

materials, like the prediction of crystal size distribution (CSD) or particle size distribution (PSD) (see e.g. [7,8]).

In a discontinuous reactor, the nucleation rate of calcium carbonate particles is related to the evolution of particle number concentration while the crystal growth rate is related to the variation of the crystal size with time. During crystal growth processes, new particles can be created by nucleation events. The rate of nucleation can play an important role on the final textural properties of the solid (e.g. specific surface area and particle size distribution.). However, this step remains the most difficult and the less studied because of the small particle size. With new developments in the measurements of sizes of fine particles, several authors attempted to study this process experimentally (e.g. [9] and references therein).

The simultaneous determination of nucleation and growth rates from batch spontaneous precipitation has been proposed by several authors (e.g. [9]). Unfortunately, this method is difficult to apply to multiphasic gas–liquid–solid or biphasic gas–solid systems under high temperature–pressure conditions because it is based on the in situ simultaneous measurements of the solution concentration (by a conductometer) and the crystal size distribution (by a laser diffraction granulometer) during a batch spontaneous precipitation (solution–solution interaction), under atmospheric pressure–temperature conditions. Recently, Montes-Hernandez et al. [10] have proposed a method to estimate the initial linear growth rate of sub-micrometric particles of calcite by using Rietveld refinements of X-ray diffraction (XRD) patterns. In that study, the calcite crystals were produced in a triphasic gas–liquid–solid system under high gas pressure (55 and 90 bar) and moderate and high temperature (30 and 90 °C). The Rietveld refinements of XRD patterns allowed estimating the variation of the coherent domain average size r [nm] with reaction time t [s]. Then, a kinetic pseudo-second-order expression was successfully used to fit the data and to determine the linear growth initial-rate of sub-micrometric particles of calcite.

The present study shows that the abovementioned method can also be used to determine the linear growth initial-rate of nanosized calcite synthesized via gas–solid carbonation of portlandite ($Ca(OH)_2$) particles in a static bed reactor. In particular, here we show that the calculated linear growth rate using the method developed in [10] is at odds with mass growth rates determined from mass variation of solid with time, using the final surface area of particles determined by BET measurements. As a consequence, such discrepancies emphasize the importance of the new method we used to obtain the kinetic data gathered in the present study, which possibly overcome the shortcomings of the mass growth rate method.

2. Experimental

2.1. Growth of nanosized calcite via gas–solid carbonation in a static bed reactor

A powder sample of 74.1 g (≈1 mol) of commercial portlandite $Ca(OH)_2$ (provided by Sigma–Aldrich with 96% of chemical purity, about 3% of $CaCO_3$ and 1% of other impurities) was placed in a titanium reactor (Parr© autoclave with internal volume of 2 L). The reactor, containing nanosized particles of portlandite, was slightly heated to 30 °C using an oven specifically fitted to the reactor. When the system temperature was stabilized, 20 bar of CO_2 (provided by Linde Gas S. A. with 99.995% of chemical purity) was injected into the static bed reactor. This pressure of CO_2 corresponds to the total initial pressure in the system. At these pressure and temperature (P–T) conditions, the vapour phase consists mainly of CO_2 gas in ideal state. To estimate the linear growth rate of calcite, five different reaction durations were considered (5, 10, 30, 90 and 180 min).

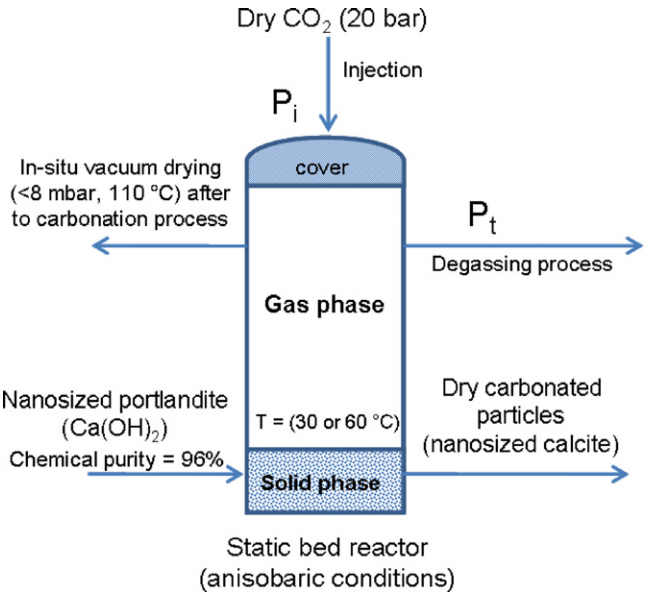

Fig. 1. Flow-chart diagram for production of nanosized calcite particles via gas–solid carbonation of nanosized $Ca(OH)_2$ particles by using a static bed reactor under anisobaric conditions (modified from Montes-Hernandez et al. [6]).

The experiments were also carried out at 60 °C and 20 bar for the same reaction durations in order to determine the effect of reaction temperature on the linear growth rate of calcite. For each experiment, when the established duration of reaction was reached, the CO_2 gas was immediately removed from the reactor by flash purge down to the atmospheric pressure. The residual CO_2 and in situ produced molecular water ($Ca(OH)_2(s) + CO_2(g) \rightarrow CaCO_3(s) + H_2O$ (v or l)) were removed from the reactor by in situ vacuum drying (<8 mbar and 110 °C) for 24 h (Fig. 1).

At the end of the experiment, i.e. after carbonation reaction, flash purge and in situ vacuum drying, the autoclave was disassembled. The dry solid product was manually recovered, weighed and stored in plastic flasks for further characterization by X-ray diffraction (XRD). For additional information on the synthesis and characterization of nanosized calcite refer to a previous study [6].

2.2. X-ray diffraction analysis of solid phase

X-ray diffraction (XRD) data were collected with a Rigaku ultraX18HFCE Bragg–Brentano diffractometer equipped with a rotating copper anode (Cu Kα radiation). The conditions for generating the X-ray beam were 300 mA and 50 kV. Scans were taken for 2θ ranges from 15° to 90° with 0.01°/s steps.

Starting material (portlandite) and carbonated powders were placed in a glass sample holder and pressed against a ground glass slide in order to avoid preferential orientation of the powder. Because of the small size of the crystallites, this process was sufficient to obtain powders with random orientation.

Rietveld refinement of XRD patterns was carried out with the program Fullprof [11], following a standard procedure [10,12,13]. Starting values for cell parameters, as well as atomic positions and atomic displacement parameters, were taken from Sitepu et al. [14] for calcite and Nagai et al. [15] for portlandite. The accuracy of the quantitative-phase analysis was estimated better than ± 3% based on the refinement of XRD patterns of standard mixtures with known proportions of calcite and portlandite. The quantitative Rietveld refinement revealed that about 3 wt% of the starting material was composed of calcite, in agreement with commercial specifications for this material.

The microstructural features of calcite and portlandite crystals were determined following the method described in Daval et al. [13]. In a first step, the contribution of the diffractometer itself to the peak broadening was calculated by performing refinement of an XRD pattern of a strain-free sample (gadolinium gallium garnet (GGG), $Gd_3Ga_5O_{12}$). This first step allowed for the determination of the instrumental resolution function (IRF) for the diffractometer. All the corresponding parameters were then kept fixed. In a second step, the XRD patterns of the reacted portlandite powders were then modelled, any further refinement thus accounting for microstructural effects only [16]. When enough calcite was present in the powder (i.e. > 15 wt %), anisotropic size broadening was modelled in terms of spherical harmonics, allowing the coherent domain average apparent size corresponding to each reciprocal lattice vector to be calculated. Coherent domain average size was calculated by averaging the resulting size of each of the reciprocal space distances measured. A schematic representation of size variation with time by using this Rietveld refinement method of XRD patterns is reported in Fig. 2.

The Cagliotti parameter U was refined to account for some isotropic strain in the Gaussian component of the peak profile. By performing refinements with different starting values of the previously described parameters an estimation of the errors and the stability of the results can be calculated. When peak broadening was not limited by instrumental resolution, errors in size were found to be ~20%; errors in strain were less than 10%. The quality of the fit between the calculated and observed diffraction-profiles was evaluated using standard indices of agreement, such as the reduced χ^2 index defined in [11]. For all refinements, the χ^2 value was smaller than 1.94, thus corresponding to reliable values of the output parameters (e.g. apparent size of each reciprocal lattice) involved in the modelling of the XRD patterns.

3. Results and discussion

3.1. General comments

In a previous study [6], it was demonstrated that nanosized $Ca(OH)_2$ particles can be completely transformed into nanosized calcite particles via gas–solid carbonation under moderate CO_2 pressure ($20 < P_{CO_2} < 40$ bar) and temperature (30–60 °C). Comparing these results with others from experiments performed on $Ca(OH)_2$ with identical grain size but at lower CO_2 pressure ($P_{CO_2} < 2$ bar) (see [17]) suggests that the gas–solid carbonation of $Ca(OH)_2$ particles was enhanced with compressed CO_2. Thus, in the present study, the mineralization of CO_2 does not form a protective carbonate layer around the reacting particles of $Ca(OH)_2$. Herein, the growth of nanosized calcite particles was preferentially observed. These previous results have also revealed that the gas–solid carbonation efficiency with compressed CO_2 was independent of CO_2 pressure when the $CO_2/Ca(OH)_2$ molar ratio was higher than 1, independent of the reaction temperature (30 and 60 °C) and independent of the initial relative humidity. These new data may therefore increase the interest to use the gas–solid carbonation of powdered portlandite with compressed CO_2 (≤40 bar) in order to produce nanosized calcite particles. The main advantage compared with aqueous precipitation methods is a simple separation of solid product from fluid phase by degassing and conventional drying processes (although it is worth noticing that agglomeration can be reduced when working with dispersions of solids in solvents and the risk of inhalation of nanopowders is avoided when working with dispersions of the particles in the solvents instead of working with dry powder). In the following paragraphs we report and discuss particularly on the linear growth rate of nanosized calcite particles, which is an essential parameter to be used in predictive models to simulate the nucleation-growth processes of minerals and other solid materials (see for example [7,8].)

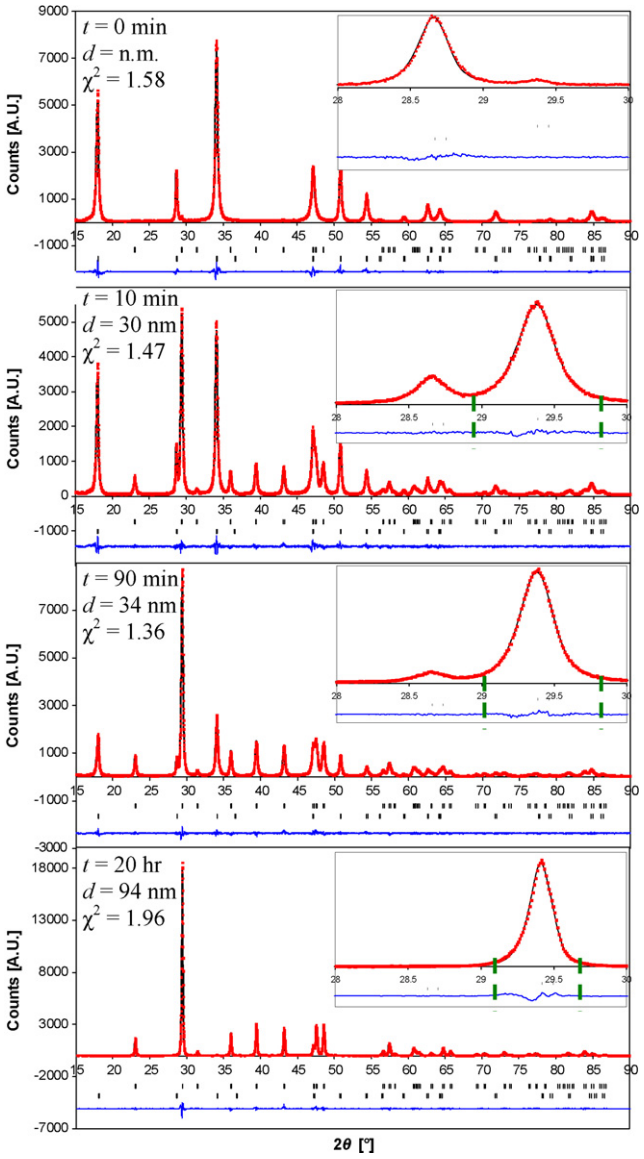

Fig. 2. Schematic representation of size variation with time by using Rietveld refinement of XRD patterns. XRD patterns of starting material ($t = 0$) and carbonated material ($t > 0$) at 30 °C and 20 bar. The red squares indicate the experimental data points of the diffractogram, the solid black line the modelled diffractogram, the solid blue line the difference between experimental and modelled diffractograms (residue). The vertical black lines indicate the positions of the Bragg reflections for each phase. (For interpretation of the references to color in this figure legend, the reader is referred to the web version of the article.)

3.2. Linear growth rate of nanosized calcite particles

For our experiments, the nucleation step was not isolated from the growth process. However, we will show below that the initial linear growth rate was estimated on a time interval where the number of newly formed calcite crystals was roughly constant, such that virtually, the system evolved with a fix amount of seeds, supposedly formed in a time duration shorter than what was experimentally reachable (i.e. ≤5 min). In such a way, we are confident that the reported measurements actually reflect the initial linear growth rate of the calcite seeds.

The ex situ measurements of the variation of crystal size with reaction time were performed by using the Rietveld refinement of

Table 1
Coherent domain average size for calcite (r) and $Ca(OH)_2$ (l) estimated by using Rietveld refinement of X-ray diffraction patterns (powder diffraction data). The error for all values is better than 10%.

P (bar)*	T (°C)	Reaction time, t (s)	r (nm)	l (nm)
		0	0	31
		300	27	27
		600	30	25
20	30	1800	31	25
		5400	34	24
		10,800	37	22
		24 h**	94	0
		0	0	31
		300	26	28
		600	27	26
20	60	1800	33	26
		5400	34	24
		10,800	36	22
		24 h**	43	0

r: Coherent domain average size for calcite; l: coherent domain average size for $Ca(OH)_2$.
* Initial CO_2 pressure into the reactor (anisobaric conditions).
** Equilibrium state, i.e. the pressure drop or CO_2 consumption by carbonation is no more detected in the system (see [6]).

each X-ray pattern. This refinement method allowed for the estimation of how the average particle size (expressed as coherent domain average size) was increasing as a function of reaction time ($r = f(t)$) (see Table 1 and Section 2.2). A sharp increase of the average size of calcite particles is initially observed, followed by a much more gradual evolution during the first 3 h of reaction (out of equilibrium) (see Fig. 3). Our strategy for determining the initial linear growth rate of calcite relies on fitting the experimental $r = f(t)$ data with an ad hoc expression, as successfully applied in previous studies [10,18,19].

The particle growth behaviour portrayed in Fig. 3 can be adequately fitted with a kinetic pseudo-second-order equation such as demonstrated in a previous study [10]. This equation was chosen because it generates suitable curves for mimicking a process consisting in a fast mass transfer followed by a slow equilibration of mass transfer in closed systems. Note that the kinetic pseudo-second-order model has been widely used to fit the experimental kinetic data of several physicochemical reactions at solid–fluid interfaces (see e.g. [18,19]). The differential form for this kinetic model can be written as follows:

$$\frac{dr}{dt} = k_G(r_{\max} - r)^2 \quad (1)$$

where k_G [1/nm s] is the rate constant of calcite-crystal growth, r_{max} [nm] is the maximum of coherent domain average size at equilibrium, r [nm] is the coherent domain average size at any time, t,.

The integrated form of Eq. (1) for the boundary conditions $t = 0$ to $t = t$ and $r = 0$ to $r = r$, is represented by a hyperbolic relationship:

$$r = \frac{r_{\max}.t}{(1/k_G.r_{\max}) + t} \quad (2)$$

Remark that the rate constant k_G has no physical interpretation. For this reason a new parameter can be defined $(1/k_G.r_{\max}) = t_{1/2}$, which represents the duration after which half of the maximum of coherent domain average size (within the considered range of time, i.e. <3 h) was obtained. In the current study, $t_{1/2}$ is called "half-growth time" and can be used to calculate the linear growth initial-rate of calcite, v_{LG} [nm/s] by using the following expression:

$$v_{LG} = \frac{r_{\max}}{t_{1/2}} = k_G(r_{\max})^2 \quad (3)$$

Table 2
Parameters for the fit of Eq. (2), linear growth initial-rate of calcite calculated by Eq. (3) and correlation factor.

T–P system (°C – bar)	r_{max} (nm)	$t_{1/2}$ (s)	v_{LG} (nm/s)	R^2
30–20	35.0 ± 1.0	98.7 ± 27.4	0.35	0.99
60–20	35.3 ± 0.9	130.0 ± 25.7	0.27	0.99

T: temperature; P: pressure; r_{max}: maximum of coherent domain average size (i.e. at equilibrium); $t_{1/2}$: half-growth time; v_{LG}: linear growth initial-rate of calcite; R^2: correlation factor.

Graphically, the linear growth initial-rate v_{LG} is defined as the slope of the tangent line when t tends towards zero on the r vs. t curve (see also: [10]).

Fitting the kinetic data (r vs. t) by using Eq. (2) allows for the estimation of the values of $t_{1/2}$ and r_{max}. Here, a non-linear regression by the least-squares method was performed. In the Fig. 3, the data and fitting curves are reported. Moreover, the fitting parameters ($t_{1/2}$ and r_{max}), the linear growth initial-rate of calcite (v_{LG}) (calculated by Eq. (3)) and the correlation factor values are summarized in the Table 2 and reported directly in the Fig. 3. These results revealed that the values of linear growth rate of calcite were roughly equivalents for two different temperatures, 0.35 nm/s at 30 °C and 20 bar and 0.27 nm/s at 60 °C and 20 bar. Moreover, the estimated average size of calcite crystals, here expressed as a maximum of

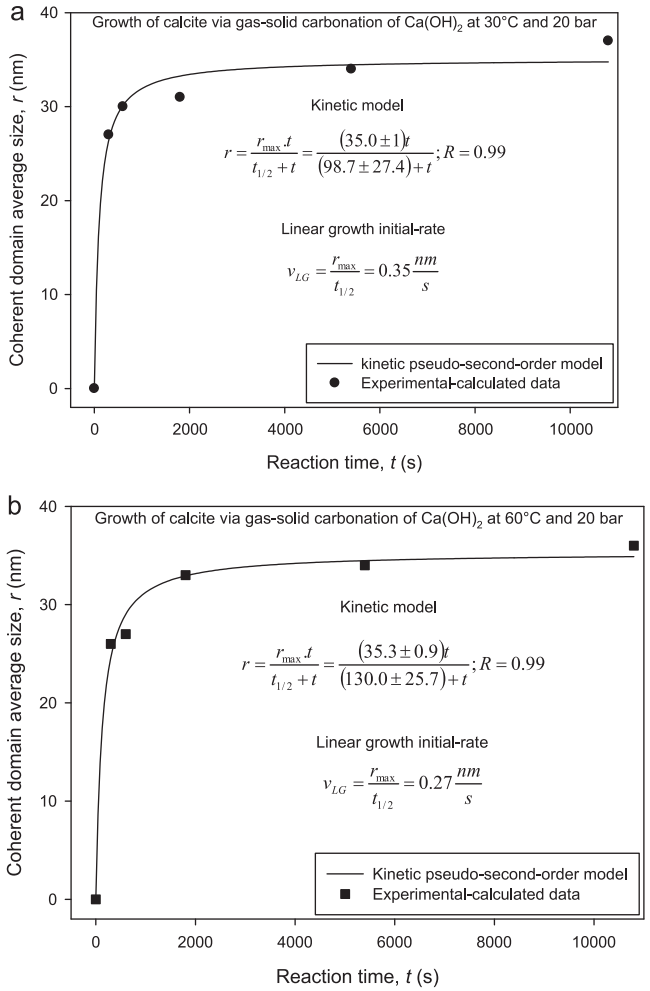

Fig. 3. Linear growth rate of calcite via gas–solid carbonation of $Ca(OH)_2$ particles under anisobaric conditions (a) at 30 °C and 20 bar, and (b) 60 °C and 20 bar. Note that the coherent domain average size was estimated by using Rietveld refinements of X-ray diffraction patterns. The fitting parameters and the linear growth rate of calcite are also reported in Table 2.

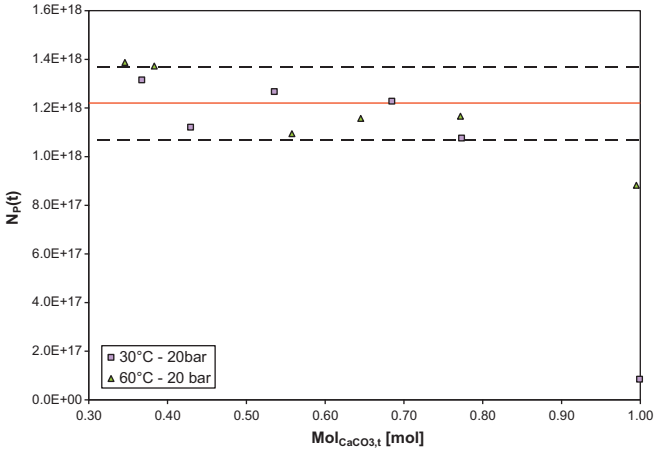

Fig. 4. Evolution of the number of formed calcite particles as a function of the extent of carbonation for both experimental conditions. The red line represents the average number of particles calculated from the data obtained for $Mol_{CaCO_3,t} < 0.8$, and the dotted lines represent the confidential interval, calculated from the propagations of errors on the parameters determined by Rietveld refinement. (For interpretation of the references to color in this figure legend, the reader is referred to the web version of the article.)

coherent domain average size after 3 h was identical for both systems, within uncertainties (35.0 ± 1.0 nm at 30 °C vs. 35.3 ± 0.9 nm). Conversely, if one was to suppose that these estimated lengths represent the equilibrium values of particle size (because of the asymptotic behaviour of the fitting curves), then we evidence that these predictions of particle size are in disagreement with data at equilibrium reported in Table 1. Here, the coherent domain average size at equilibrium (after 24 h of reaction) is clearly higher for both temperatures, 94 ± 9 nm at 30 °C and 20 bar and 43 ± 4 nm at 60 °C and 20 bar (see also: [6]). Moreover, note that any model (simple pseudo-first or second-order) would have failed to describe the whole range of data from 0 to 24 h.

This result suggests in turn that a supplementary process took place for extents of carbonation greater than 80%. The mechanisms responsible for such discrepancies may be better understood by estimating roughly the mean number of calcite particles at any time throughout carbonation. If one considers, for the sake of simplicity, that all crystallites consist in spheres, then the total amount of particles at a given extent of reaction $N_p(t)$ is given by:

$$N_p(t) = \frac{6M_{CaCO_3}.Mol_{CaCO_3,t}}{\pi \rho_{CaCO_3} r^3} \quad (4)$$

where M_{CaCO_3}, $Mol_{CaCO_3,t}$, ρ_{CaCO_3} and r are respectively the molar mass [g/mol], the amount [mol], the specific gravity [g/cm^3] and the coherent domain average size [cm] of calcite at any time. The results are shown in Fig. 4. A first striking point is that, for $Mol_{CaCO_3,t} < 0.8$, the number of calcite particles is roughly constant, within experimental uncertainties, all along the carbonation process for both experiments. This result ensures that a linear growth rate was computable on the corresponding time interval, without (or with only minor) interferences by other processes such as secondary nucleation events. Conversely, $N_p(t)$ decreases dramatically for $Mol_{CaCO_3,t} > 0.8$ (about one order of magnitude of discrepancies for the experiment carried out at 30 °C). Such a result implies that for an extent of carbonation comprised between 0.8 and 1.0, the calcite nuclei undergo a complex evolution (possibly, by dissolution–reprecipitation, see below), where some of the seeds keep growing at the expense of the others, which tend to disappear. Note that such features had already been evidenced for the aqueous carbonation of portlandite (e.g. [10,12]). Note also that such a process may have a huge impact when determining initial linear growth rate of calcite by using physical properties of reaction products determined for $Mol_{CaCO_3,t} > 0.8$, which is the case with the mass growth rate method (see Section 3.3).

A possible explanation for this complex process, which becomes really significant at high extent of carbonation only (>0.8) and which, as a consequence, does not invalidate the previous fitting realized for an extent of carbonation <0.8, is that the calcite dissolution step could be linked to the release of water into the reactor during the reaction: $Ca(OH)_2(s) + CO_2(g) \rightarrow CaCO_3(s) + H_2O$ (v or l). Such a release may have an impact on the stability of the calcite nuclei only when there is enough water to dissolve CO_2, implying local acidic conditions and subsequent calcite dissolution.

3.3. Mass growth rate of nanosized calcite particles

The mass growth rate can be defined as the global mass flux incorporated and/or nucleated at solid–fluid interfaces during crystal growth processes. This mass flux can be related to the particle size in order to deduce the linear growth rate (e.g. [9,20,21]), assuming that secondary nucleation events are insignificant during growth processes. This concept was suitable to our measurements. For this case, the carbonation extent as a function of time was calculated using a simple mass balance method, based on the theoretical overall carbonation reaction. Herein, the carbonation extent (CE_t) at any established reaction time was then calculated by the following equation:

$$CE_t = \frac{w_{dry-product,t} - w_{Ca(OH)_2(initial)}}{w_{theoretical} - w_{Ca(OH)_2(initial)}} \quad (5)$$

where $w_{dry-product,t}$ [g] is the experimental mass of dry solid product at any time, t (in situ vacuum drying (<8 mbar and 110 °C)), $w_{theoretical}$ [g] is the theoretical mass of calcium carbonate [considering 100% of carbonation ($Ca(OH)_2$–$CaCO_3$ transformation), $w_{Ca(OH)_2(initial)}$ [g] is the initial mass of calcium hydroxide loaded in the reactor. Consequently, the unreacted calcium hydroxide in the solid product [g] as a function of time was calculated by:

$$w_{Ca(OH)_2(unreacted),t} = w_{Ca(OH)_2(initial)} - w_{Ca(OH)_2(initial)} \times CE_t \quad (6)$$

Then, the amount of calcite [g] at any given time was calculated by a simple mass balance:

$$w_{CaCO_3(growth),t} = w_{dry\_product} - w_{Ca(OH)_2(unreacted),t} \quad (7)$$

All the temporal values calculated by Eqs. (5)–(7) are summarized in Table 3. Particularly, the amount of calcite as a function of time was used to determine the mass growth rate of calcite. To reach this goal, a kinetic pseudo-second-order equation was also used because the amount of calcite increased sharply with time first and was followed by a slower step during the first 3 h of reaction (out-equilibrium) (see data in Fig. 5). For this case, the differential form for kinetic pseudo-second-order expression can be written as follows:

$$\frac{d[Mol_{CaCO_3,t}]}{dt} = k_{n-g}(Mol_{CaCO_3,max} - Mol_{CaCO_3,t})^2 \quad (8)$$

where k_{n-g} [1/mol s] is the rate constant of calcite formation for a given initial amount of $Ca(OH)_2$, $Mol_{CaCO_3,max}$ [mol] is the maximum amount of calcite at equilibrium, $Mol_{CaCO_3,t}$ [mol] is the formed amount of calcite at any time, t.

The integrated form of Eq. (8) for the boundary conditions $t = 0$ to $t = t$ and $Mol_{CaCO_3,t} = 0$ to $Mol_{CaCO_3,t} = Mol_{CaCO_3,t}$, is expressed by the following hyperbolic equation:

$$Mol_{CaCO_3,t} = \frac{(Mol_{CaCO_3,max})t}{t^*_{1/2} + t} \quad \text{where} \quad t^*_{1/2} = \frac{1}{(k_{n-g})(Mol_{CaCO_3,max})} \quad (9)$$

Table 3
Mass variation of calcite and $Ca(OH)_2$ during gas–solid carbonation process estimated by a simple mass balance method (see Eqs. (5)–(7)). The error for all values is better than 5%.

P (bar)*	T (°C)	t (s)	$w_{dry-product,t}$ (g)	CE_t	$w_{Ca(OH)_2(unreacted),t}$ (g)	$w_{CaCO_3(growth),t}$ (g)
20	30	0	74.10	0	74.10	0
		300	83.08	0.34	48.49	34.58
		600	84.60	0.40	44.16	40.43
		1800	88.34	0.54	33.50	54.83
		5400	91.82	0.68	23.57	68.24
		10800	93.70	0.75	18.21	75.48
		24 h**	99.12	0.96	2.76	96.35
20	60	0	74.10	0	74.10	0
		300	81.85	0.29	52.00	29.84
		600	83.31	0.35	47.84	35.46
		1800	87.41	0.51	36.15	51.25
		5400	89.97	0.61	28.85	61.11
		10800	92.43	0.70	21.83	70.59
		24 h**	99.13	0.96	2.73	96.39

* Initial CO_2 pressure into the reactor (anisobaric conditions).
** Equilibrium state, i.e. the pressure drop or CO_2 consumption by carbonation is not more detected in the system (see [6]).

Physically the parameter $t^*_{1/2}$ represents the time after which half of the maximum amount of calcite was obtained, within the considered time interval (i.e. <3 h). In the current study, $t^*_{1/2}$ is called "half-formation time for calcite" and is used to calculate the mass growth initial-rate of calcite, v_{MG}, [mol/s] by the following expression:

$$v_{MG} = \frac{\mathrm{Mol}_{CaCO_3,\max}}{t^*_{1/2}} = k_{n-g}(\mathrm{Mol}_{CaCO_3,\max})^2 \quad (10)$$

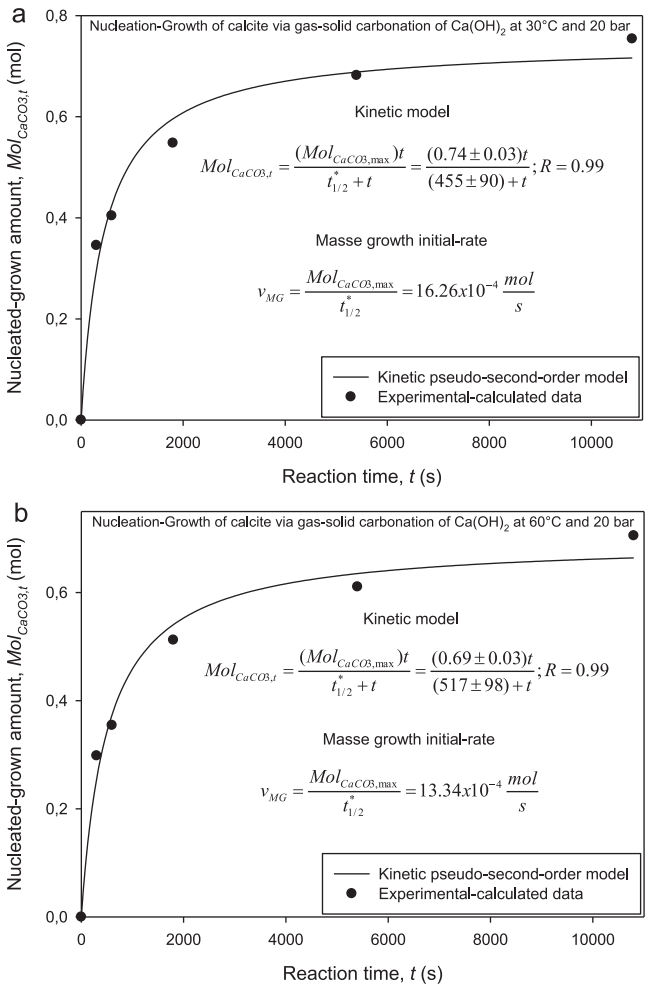

Fig. 5. Mass growth rate of calcite via gas–solid carbonation of $Ca(OH)_2$ particles under anisobaric conditions (a) at 30 °C and 20 bar, and (b) 60 °C and 20 bar. The fitting parameters and the mass growth rate of calcite are also reported in Table 4.

The fit of the kinetic data ($\mathrm{Mol}_{CaCO_3,t}$ vs. t) using Eq. (9) is shown in Fig. 5. The parameters $t^*_{1/2}$ and $\mathrm{Mol}_{CaCO_3,\max}$ were estimated by applying non-linear regression by the least squares method. These two fitting parameters, the mass growth initial-rate of calcite (v_{MG}) (calculated by Eq. (10)) and the correlation factor values are summarized in the Table 4 and reported directly in the Fig. 5. These results revealed that the values of mass growth rate of calcite were also equivalent for both systems, 16.3×10^{-4} mol/s at 30 °C and 20 bar, and 13.3×10^{-4} mol/s at 60 °C and 20 bar. In summary, the fitting strategy we used describes correctly the experimental kinetic data for reaction time ranging from 0 to 3 h, but the corresponding equilibrium parameters ($\mathrm{Mol}_{CaCO_3,\max} = 0.74$ (30 °C; 20 bar) and 0.69 (60 °C, 20 bar)) are in significant disagreement with experimental measurements corresponding to the achievement of a macroscopic equilibrium (24 h of reaction) (i.e. complete $Ca(OH)_2$-to-calcite transformation, where $\mathrm{Mol}_{CaCO_3}(t = 24h) = 1$, see [6]).

In order to solve this fitting problem, two kinetic regimes during carbonation process should be assumed. This assumption fitting implies a more complex physical explanation of kinetic behaviour and additional fitting parameters. The physical explanation could imply the complex process proposed above: (1) dry to wet carbonation for extent of carbonation < 0.8 and then (2) aqueous carbonation of portlandite for extent of carbonation > 0.8, in which calcite nuclei undergo a dissolution step followed by a growth step of the remaining nuclei. This later reaction could follow an Ostwald ripening-like mechanism, where only the biggest calcite nuclei keep on growing, at the expense of the smallest. For example, one can assume a double kinetic pseudo-second-order model (i.e. two kinetic regimes), for which the integrated form is given by the following hyperbolic equation:

$$\mathrm{Mol}_{CaCO_3,t} = \frac{(\mathrm{Mol}_{CaCO_3,\max_1})t}{t^*_{1/2a} + t} + \frac{(\mathrm{Mol}_{CaCO_3,\max_2})t}{t^*_{1/2b} + t} \quad (11)$$

Obviously, a better fitting was found with this kinetic formulation (Eq. (11)) and a realistic $Ca(OH)_2$-to-$CaCO_3$ molar transformation at equilibrium was also estimated (see Fig. 6, corresponding to the experiment performed at 30 °C).

Table 4
Parameters for the fit of Eq. (9), mass growth initial-rate of calcite calculated by Eq. (10) and correlation factor.

T–P system (°C – bar)	$Mol_{CaCO_3,max}$ (mol)	$t_{0.5}$ (s)	v_{MG} (mol/s)	R^2
30–20	0.74 ± 0.03	455 ± 90	16.3×10^{-4}	0.99
60–20	0.69 ± 0.03	517 ± 98	13.3×10^{-4}	0.99

T: temperature; P: pressure; $Mol_{CaCO_3,max}$: maximum amount of calcite (i.e. at equilibrium) according to the fit of the data; $t_{0.5}$: half-growth time; v_{MG}: mass growth initial-rate of calcite; R^2: correlation factor.

Table 5
Summary of growth rate values, calcite weight and specific surface area of calcite synthesized at 30 °C and 20 bar, and at 60 °C and 20 bar via gas–solid carbonation of $Ca(OH)_2$ particles under anisobaric conditions.

T–P system (°C – bar)	v_{MG} (mol/s)	$S_{BET\_product}$ (m^2/g)	m_{CaCO_3} (g)	$v_{MG\rightarrow LG}$ (nm/s)	v_{LG} (nm/s)
30–20	16.3×10^{-4}	7.0	96.3	0.089	0.35
60–20	13.3×10^{-4}	8.1	96.4	0.063	0.27

v_{MG}: mass growth rate (see Fig. 5 in this study); $S_{BET\_product}$: specific surface area of product at equilibrium state (see [6]); m_{CaCO_3}: formed calcite weight at equilibrium; $v_{MG\rightarrow LG}$: linear growth rate of calcite deduced from mass growth rate (see Eq. (12)); v_{LG}: linear growth rate deduced from Rietveld refinement of XRD patterns (see Section 3.2).

Finally, the linear growth rate of calcite from mass growth rate can be deduced as follows:

$$v_{MG\rightarrow LG} = \frac{M_{CaCO_3}}{\rho_{CaCO_3} S_{BET\_product} m_{CaCO_3}} v_{MG} \quad (12)$$

where M_{CaCO_3}, ρ_{CaCO_3} and m_{CaCO_3} are the molar mass, the density and the produced weight of calcite, respectively. The $S_{BET\_product}$ is the specific surface area of product and it is equivalent to specific surface area of calcite in our experiments, assuming a complete transformation of calcium hydroxide ($Ca(OH)_2$) to calcite ($CaCO_3$). Table 5 summarizes the growth rate values, the produced weight and the specific surface areas of calcite synthesized at 30 °C and 20 bar, and at 60 °C and 20 bar.

Note that the Eq. (12) represents only an "a posteriori" calculation, knowing the specific surface area of solid product and the produced calcite weight at the equilibrium. This global calculation does not take into account the temporal variation of the specific surface area of solid during calcite-crystal growth, which could represent a major shortcut in the treatment of the data. However, despite this assumption, it has been previously shown that such a calculation could be a relevant approximation to deduce the linear growth rate (see [10]).

Conversely, in this present study a significant discrepancy was found: the estimated values from this indirect method were about 4 times smaller than linear growth rates estimated by a direct method (i.e. estimation of coherent domain average size as a function of time by Rietveld refinement of XRD patterns). Fig. 7 shows the discrepancy of linear growth rate values with respect to the theoretical line (with slope = 1). Several explanations could account for such discrepancies such as agglomeration processes of the calcite crystals or dissolution–reprecipitation events which occurred at the very end of the reaction. As a consequence, these processes make challenging the extrapolation of kinetic parameters for linear growth rate of calcite using the latter approach, such that this method most likely fails in providing reliable linear growth rate data. As emphasized in Section 3.2, the use of parameters extrapolated at the very end of the reaction (such as the specific surface area of the powder), whose state is not representative of that of the products during the initial growth stage, could be the main source of errors in the treatment of the data following this second approach.

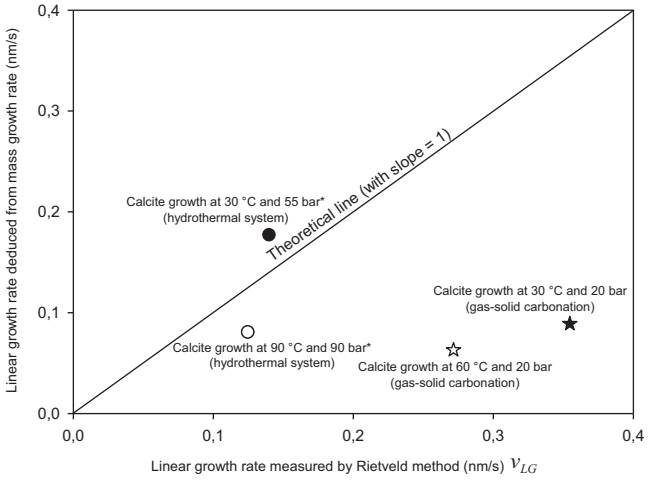

Fig. 7. Comparison of linear growth rate values deduced from mass growth rate with linear growth rate values deduced by the average variation of crystal size (i.e. variation of coherent domain average size) as a function of reaction time. Coherent domain average size was determined by Rietveld refinement of X-ray diffraction patterns. Circles indicate experiments in which calcite was synthesized in a triphasic gas–liquid–solid system under hydrothermal conditions (see [10]).

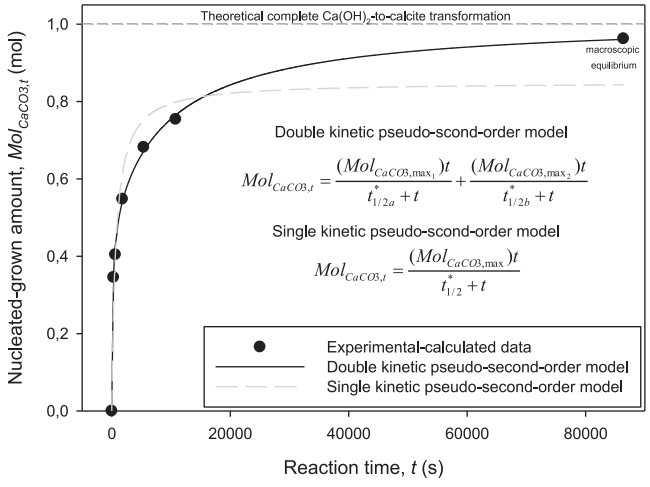

Fig. 6. Fit of the kinetic experimental data for 30 °C and 20 bar system by assuming two kinetic regimes (double kinetic pseudo-second-order expression). A better fit was found compared to single kinetic model and a realistic $Ca(OH)_2$-to-$CaCO_3$ molar transformation at equilibrium was also estimated.

4. Conclusion

The main goal for this study was to apply two independent methods in order to estimate how particle size of calcite was increasing with reaction time. Firstly, a direct method by using Rietveld refinements of X-ray diffraction (XRD) patterns was applied to determine the variation of the coherent domain average size r [nm] with reaction time t [s]. Second, we used a mass

balance method where the calcite amount $Mol_{CaCO_3,t}$ [mol] was determined as a function of time t [s] and the linear growth rate was deduced from mass growth rate. To the best of our knowledge, here we reported for the first time data on the linear growth rate of nanosized calcite particles synthesized via gas–solid carbonation of nanosized $Ca(OH)_2$ particles under anisobaric conditions. Note that the linear growth initial-rate is an essential parameter to be used in predictive models to simulate the nucleation-growth processes of minerals and solid materials. Specifically, the data extrapolated from the present study could be useful to extrapolate the growth rate of calcite particles in biphasic (gas–solid) systems where water, a by-product of the reaction we studied, would be continuously removed.

The main advantage for these methods is that they make possible the estimation of linear growth rate of crystalline fine particles growing in multiphasic fluid–solid (including gas–solid reactions) systems under high pressure and temperature. However, the complex processes affecting the fate of calcite nuclei for high extent of carbonation (>0.8 according to the experimental results of the present study), in relation with the release of molecular water, was measured to modify considerably the equilibrium size, and possibly the agglomeration state, of calcite particles at the very end of the reaction. This latter process can be suggested to modify potentially the specific surface area of the final calcite, thus making challenging the use of a simple mass growth balance method. As a consequence, such complex effects emphasize that the use of alternative techniques, such as the one described in this study using Rietveld refinements of XRD patterns, should be preferred in future to studies to obtain more accurate and reliable linear-growth rate data.

Acknowledgements

The authors are grateful to French National Center for Scientific Research (CNRS) and University Joseph Fourier (UJF) in Grenoble for providing the financial support.

References

[1] V. Prigiobbe, A. Polettini, R. Baciocchi, Gas–solid carbonation kinetics of air pollution control residues for CO_2 storage, Chem. Eng. J. 148 (2009) 270–278.
[2] S. Stendardo, P.U. Foscolo, Carbon dioxide capture with dolomite: a model for gas–solid reaction within the grains of a particulate sorbent, Chem. Eng. Sci. 64 (2009) 2343–2352.
[3] P. Sun, J.R. Grace, C.J. Lim, E.J. Anthony, A discrete-pore-size-distribution-based gas–solid model and its application to the $CaO + CO_2$ reaction, Chem. Eng. Sci. 63 (2008) 57–70.
[4] D.N. Huntzinger, J.S. Gierke, S.K. Kawatra, T.C. Eisele, L.L. Sutter, Carbon dioxide sequestration in cement kiln dust through mineral carbonation, Environ. Sci. Technol. 43 (2009) 1986–1992.
[5] M. Fernandez Bertos, S.J.R. Simons, C.D. Hills, P.J. Carey, A review of accelerated carbonation technology in the treatment of cement-based materials and sequestration of CO_2, J. Hazard. Mater. B112 (2004) 193–205.
[6] G. Montes-Hernandez, D. Daval, R. Chiriac, F. Renard, Growth of nanosized calcite through gas–solid carbonation of nanosized portlandite under anisobaric conditions, Cryst. Growth Design 10 (2010) 4823–4830.
[7] B. Fritz, C. Noguera, Mineral precipitation kinetics, Rev. Min. Geochem. 70 (2009) 371–410.
[8] B. Fritz, A. Clement, Y. Amal, C. Noguera, Simulation of the nucleation and growth of simple clay minerals in weathering processes: the NANOKIN code, Geochim. Cosmochim. Acta 73 (2009) 1340–1358.
[9] M. Aoun, E. Plasari, R. David, J. Villermaux, A simultaneous determination of nucleation and growth rates from batch spontaneous precipitation, Chem. Eng. Sci. 54 (1999) 1161–1180.
[10] G. Montes-Hernandez, A. Fernandez-Martinez, F. Renard, Novel method to estimate the linear growth rate of submicrometric calcite produced in a triphasic gas–liquid–solid system, Cryst. Growth Design 9 (2009) 4567–4573.
[11] J. Rodriguez-Carvajal, An introduction to the program FullProf.2k. (2010) http://www.ill.eu/sites/fullprof/php/tutorials.html.
[12] G. Montes-Hernandez, A. Fernandez-Martinez, L. Charlet, D. Tisserand, F. Renard, Textural properties of synthetic calcite produced by hydrothermal carbonation of calcium hydroxide, J. Cryst. Growth 310 (2008) 2946–2953.
[13] D. Daval, I. Martinez, J-M. Guigner, R. Hellmann, J. Corvisier, N. Findling, C. Dominici, B. Goffé, F. Guyot, Mechanism of wallostonite carbonation deduced from micro- to nanometer length scale observations, Am. Mineral. 94 (2009) 1707–1726.
[14] H. Sitepu, B.H. O'Connor, D. Li, Comparative evolution of the March and generalized spherical harmonic preferred orientation models using X-ray diffraction data for molybdyte and calcite powders, J. Appl. Crystallogr. 38 (2005) 158–167.
[15] T. Nagai, T. Ito, T. Hattori, T. Yamanaka, Compression mechanism and amorphization of portlandite, $Ca(OH)_2$ structural refinement under pressure, Phys. Chem. Miner. 27 (2000) 462–466.
[16] D. Martinez-Blanco, P. Gorria, J.A. Blanco, M.J. Perez, J. Campo, Analysis of the diffraction-line broadening on nanostructured Fe: size-strain effects induced by milling and heating, J. Phys.: Condens. Mater. 20 (2008), 335213 (10pp).
[17] G. Montes-Hernandez, A. Pommerol, F. Renard, P. Beck, E. Quirico, O. Brissaud, In situ kinetic measurements of gas–solid carbonation of $Ca(OH)_2$ by using an infrared microscope coupled to a reaction cell, Chem. Eng. J. 161 (2010) 250–256.
[18] G. Montes-Hernandez, S. Rihs, A simplifed method to estimate kinetic and thermodynamic parameters on the solid–liquid separation of pollutants, J. Colloid Interface Sci. 299 (2006) 49–55.
[19] G. Montes-H, Y. Geraud, Sorption kinetic of water vapour of MX80 bentonite submitted to different physical–chemical and mechanical conditions, Colloids Surfaces A 235 (2004) 17–23.
[20] P.C. Chen, C.Y. Tai, K.C. Lee, Morphology and growth rate of calcium carbonate crystals in a gas–liquid–solid reactive crystallizer, Chem. Eng. Sci. 52 (1997) 4171–4177.
[21] A.E. Nielsen, The kinetics of crystal growth in barium sulphate precipitation, Acta Chem. Scand. 12 (1958) 951–958.